第 52 卷 第 1 期/2025 年 1 月/中国激光

封面文章·研究论文

中国激光

# 飞秒激光直写多芯FBG及耦合波导的二维矢量位移传感研究

樊宇[1,2,3]，包维佳[1,2,3*]，廖常锐[1,2,3]，王义平[1,2,3,4]

[1]深圳大学射频异质异构集成全国重点实验室，广东 深圳 518060；

[2]深圳大学广东省光纤传感技术粤港联合研究中心，广东 深圳 518060；

[3]深圳大学深圳市超快激光微纳制造重点实验室，广东 深圳 518060；

[4]人工智能与数字经济广东省实验室（深圳），广东 深圳 518107

**摘要** 提出了一种利用单通道测量多路信号的多芯光纤布拉格光栅(FBG)二维矢量位移传感结构，该传感结构的主体基于飞秒激光直写技术制备。通过在多芯光纤的中间芯和侧芯中分别刻写FBG，并进一步制备能够连接中间芯与侧芯的直耦合波导，可以实现单个纤芯复用多路传感光信号的功能，因此能够避免扇入扇出器件的使用。基于该传感结构，进行了方向角为0°～360°的二维矢量位移传感测试，对方向角的测试结果进行了计算重构，并比较了实际施加角度与计算重构角度之间的误差。另外，测试了传感器在不同位移量下的方向响应，结果表明传感器的方向响应始终呈近似正弦分布。最后，测试了传感器在不同方向角下的位移响应，得到最大位移灵敏度为0.28 nm/mm。

**关键词** 矢量位移传感；飞秒激光直写；多芯光纤；光纤布拉格光栅；波导

**中图分类号** TN249 **文献标志码** A **DOI**：10.3788/CJL240941

## 1 引　　言

光纤型矢量弯曲/位移传感器具有可柔性传输、体积小巧、抗电磁干扰和生物相容性好等优点，在智能机械、形状监测、裂纹生长监测等领域中有着广泛的应用[1-7]。近年来，国内外研究学者提出了各种基于光纤弯曲来实现位移测量的紧凑型传感器件，并且这些器件表现出了优异的性能。例如，通过在光纤中引入各种非对称的结构，比如倾斜光纤光栅[8]、偏芯光纤光栅[9]、离轴光纤光栅[10]、正交光纤光栅[11]，或者利用特殊结构的光纤，比如偏芯光纤[12]、表面芯光纤[13]、D型光纤[14]、光纤干涉仪[15]，可以打破光纤的圆对称性，从而实现矢量位移传感。在众多光纤型位移传感结构中，光纤光栅型位移传感结构由于其结构简单、测量范围广、测量精度高等优点，成为近年来位移传感领域的研究热点[16]。根据光纤光栅基本类型的不同，其主要分为光纤布拉格光栅(FBG)型位移传感结构[8-11]和长周期光纤光栅(LPFG)型位移传感结构[17-18]。其中，多芯光纤光栅型(包括多芯FBG型[19-22]及多芯LPFG型[23-24])矢量位移传感结构由于有着能够多维度测量及灵敏度、分辨率和精度高等优点，近年来成为矢量位移传感器领域中的研究热点。然而，在多芯光纤光栅型矢量位移传感器的实际应用中，往往不可避免地需要使用扇入扇出器件以实现多路信号解调。该器件的使用不仅给光纤的拼接、熔接增加了难度，降低了传感器的紧凑性，还提升了系统的成本和复杂性，降低了解调效率，给现有的多芯光纤光栅型矢量位移传感器的实际应用带来了挑战。

近年来，飞秒激光直写技术被广泛应用在光纤等载体中制造各种微结构[25-31]，其中包括FBG[25-27]和折射率耦合波导[28-30]。利用该技术既可以较容易地在各种光纤中制备FBG，也可以在光纤无损的情况下，利用其折射率改性的特点，在光纤内部制造用于导光的耦合波导通道。

本文提出了一种基于飞秒激光直写多芯FBG及耦合波导的单通道测量二维矢量位移传感结构。利用飞秒激光直写技术，在七芯光纤的中间芯和两个侧芯中写入了FBG，并制备了能够使光信号在中间芯和侧芯中来回传输的耦合波导，从而仅使用一个环形器即同时测量了多个通道的光信号，改变了传统扇入扇出器件的使用方式，实现了传感组件的高度集成。另外，

**收稿日期**：2024-06-06；**修回日期**：2024-07-16；**录用日期**：2024-08-19；**网络首发日期**：2024-08-28

**基金项目**：国家自然科学基金(62122057，62075136)、广东省基础与应用基础研究基金(2022B1515120061)、深圳市科技计划(ZDSYS20220606100405013)、中核集团领创基金

**通信作者**：*wjbao@szu.edu.cn

基于该传感结构，进行了 0°～360°的二维矢量位移传感测试，对方向角测试结果进行了计算重构，并比较了实际施加角度与计算重构角度之间的误差。最后，研究了传感结构在不同位移量下的方向响应以及在不同方向角下的位移变化。该传感结构均表现出了预期的良好响应效果。

## 2 实验装置与原理

图 1 为利用飞秒激光直写技术在七芯光纤里制备 FBG 和耦合波导的示意图。该结构基于课题组自行搭建的飞秒激光直写加工系统[21]制备，所使用的飞秒激光波长为 515 nm，脉宽为 195 fs，重复频率为 1 Hz～1 MHz。激光经过显微物镜聚焦在光纤中，光纤被固定在一个组装的高精度气浮三维位移平台上，可以在 $x$、$y$、$z$ 三个维度进行精密移动。在制备过程中，通过电荷耦合器件（CCD）对光纤进行成像，便于实时观察。通过该加工系统，在七芯光纤的中间芯（core 1）以及两个方位角为 60°的侧芯（core 2 和 core 3）中制备了 FBG，并刻划了两条从 core 1 到 core 2 以及从 core 1 到 core 3 的具有一定倾斜角度（$\theta$）的直耦合波导。如图 2 所示，通过简单地将单模光纤（SMF）的纤芯与七芯光纤（MCF）的中间芯熔接，光信号即可从中间芯通过波导传输到侧芯中，在经过 FBG 的反射后，再次通过波导返回至中间芯，最终反射回单模光纤中。一旦 FBG 的反射信号由于光纤发生弯曲等而变化，则可以通过单模光纤中传输回来的光进行解调，从而获得低成本、低复杂度和高紧凑性的光纤矢量位移传感结构。

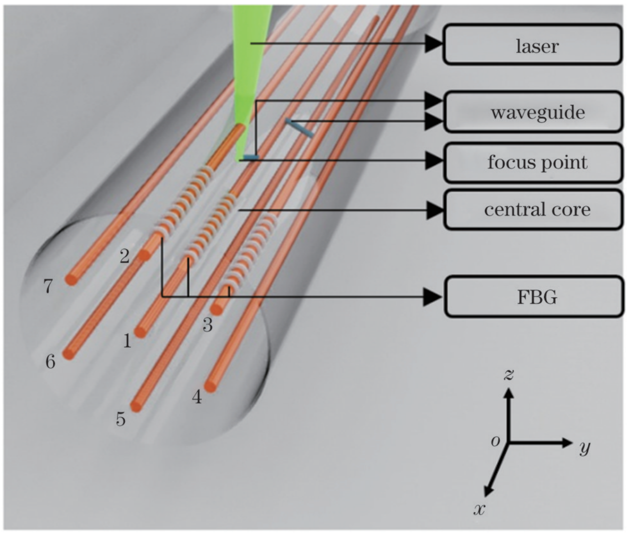


图 1 飞秒激光直写七芯 FBG 及耦合波导示意图

Fig. 1 Schematic diagram of femtosecond laser direct writing FBG and coupled waveguides in seven-core fiber

图 3(a)展示了用于制备矢量位移传感结构的七芯光纤的截面结构，其包括一个中间芯（core 1）和六个侧芯（core 2～core 7），每个纤芯的直径均为 9 μm，包层直径为 150 μm，每个相邻侧芯的方位角相差 60°，侧芯到中间芯的距离 $d$ 均为 42 μm，其中 $\theta_d$ 和 $\theta_i$（$i$=2，3，…，7）分别为弯曲方向和第 $i$ 个侧芯相对于 0°基准平面的角度。图 3(b)展示了该七芯光纤的实物端面显微图。

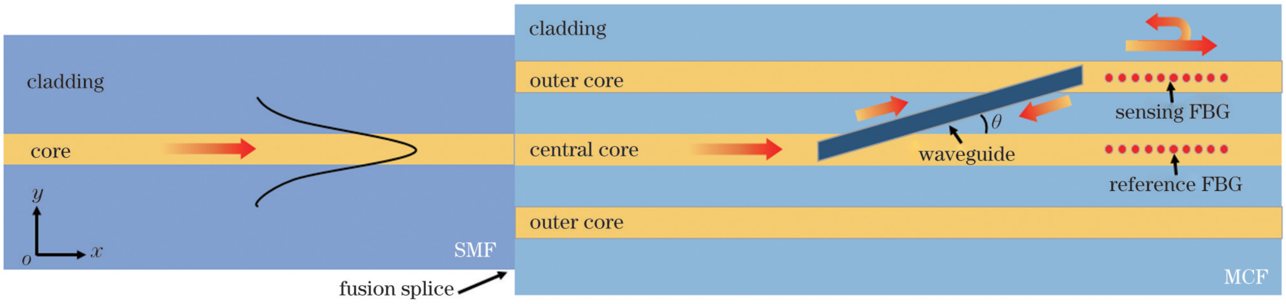


图 2 基于多芯 FBG 及耦合波导的单通道测量位移传感结构原理示意图

Fig. 2 Schematic diagram of single-channel measuring displacement sensing structure based on multi-core FBG and coupled waveguide

基于多芯 FBG 的矢量位移传感结构的基本原理是监测光纤位移（弯曲）发生时不同芯内 FBG 的布拉格波长漂移。当光纤发生弯曲时，位于弯曲外侧和内侧的 FBG 将分别被拉伸和压缩，因此导致其反射波长分别发生红移和蓝移，而中间芯的横向位置由于始终位于应变的中间面上，因此对弯曲不敏感。故位于中间芯 core 1 的 FBG 可以用于温度补偿。

对于 FBG 而言，径向应变造成的影响相对来说较为微弱，因此通常只考虑其发生的轴向应变。在线性弹性范围内，材料理论[32]定义的 FBG 轴向应变为 $\varepsilon=\frac{\Delta L}{L}$，其中 $\Delta L$ 为光纤的长度变化，$L$ 为光纤的原始长度。在恒温下发生应变时，多芯 FBG 的布拉格波长漂移[33] $\Delta\lambda_i$ 可以表示为

$$\Delta\lambda_i=\left(1-p_e\right)\lambda_i\cdot\varepsilon_i \tag{1}$$

式中：$\lambda_i$ 为第 $i$ 个侧芯中 FBG 的原始波长；$p_e$ 为有效弹光系数；$\varepsilon_i$ 为第 $i$ 个侧芯中 FBG 受到的应变，其可以进一步表示为

$$\varepsilon_i=\frac{d_i}{R}\sin\left(\theta_d+\theta_i\right) \tag{2}$$

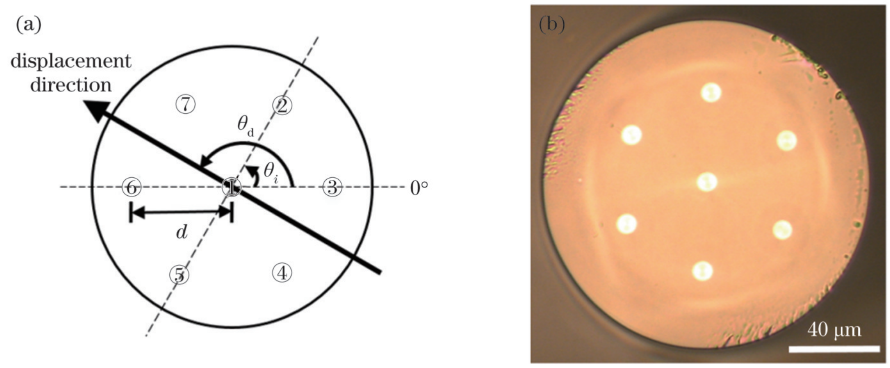


图 3　七芯光纤截面的理论模型与实际图像。(a)具有定义几何参数的七芯光纤的截面；(b)七芯光纤端面显微图

Fig. 3　Theoretical model and actual image of cross section of seven-core fiber. (a) Cross section of seven-core fiber with defined geometrical parameters; (b) cross-sectional microscopic image of seven-core fiber

式中：$d_i$为第$i$个侧芯（即 core 2～core 7）与中间芯 core 1 的中心距离；$R$为弯曲半径。在这里，由于$\theta_2$和$\theta_3$分别为 60°和 0°，距离$d$始终不变且$R \gg d$，因此，弯曲（位移）角度$\theta_d$可以最终表示为

$$\theta_d = \arctan\left(\frac{\frac{\Delta\lambda_3}{\lambda_3}\sin\theta_2 - \frac{\Delta\lambda_2}{\lambda_2}\sin\theta_3}{\frac{\Delta\lambda_2}{\lambda_2}\cos\theta_3 - \frac{\Delta\lambda_3}{\lambda_3}\cos\theta_2}\right) \tag{3}$$

一旦通过两个 FBG 的波长变化关系确定了位移的方向，便可以进一步通过各 FBG 的波长漂移量来确定位移量的大小，从而实现二维矢量位移传感。

## 3　实验结果与讨论

### 3.1　FBG 与耦合波导的制备

如图 4(a)所示，基于上述飞秒激光加工系统，在七芯光纤的中间芯（core 1）制备了参考 FBG（以下简称 FBG1），在两个夹角为 60°的侧芯（core 2 和 core 3）中分别制备了传感 FBG（以下简称 FBG2 和 FBG3），并分别制备了从 core 1 到 core 2 以及从 core 1 到 core 3 的耦合波导（以下简称波导 2 和波导 3）。其中，FBG 基于逐点法制备，长度均为 5 mm；耦合波导基于逐行扫描法制备，每个波导是由平行刻划的多条间距为 0.3 μm 的调制线叠加形成的。为了尽可能减小传输损耗，波导相

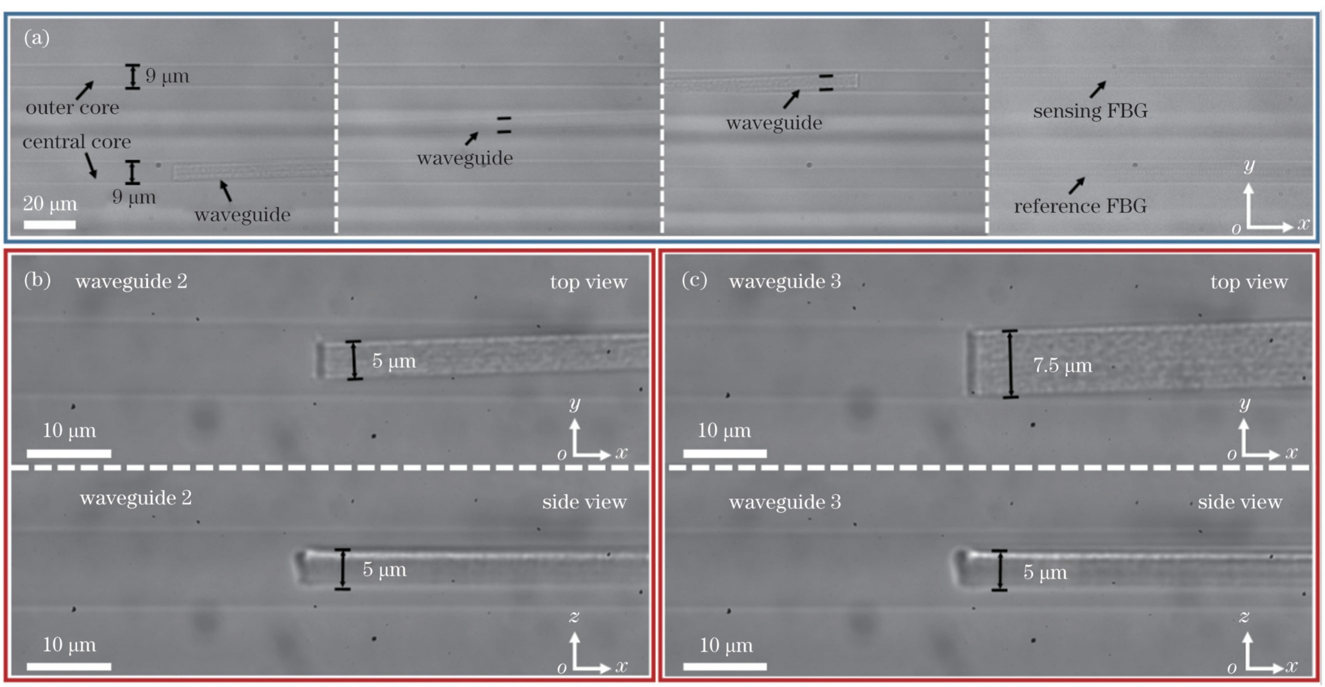


图 4　飞秒激光直写七芯 FBG 及耦合波导的显微图像。(a)$x$、$y$方向上的整体分布；(b)波导 2 的俯视及侧视形貌；(c)波导 3 的俯视及侧视形貌

Fig. 4　Microscopic images of femtosecond laser direct writing FBGs and coupled waveguides in seven-core fiber. (a) Overall distributions in $x$ and $y$ directions; (b) top and side view morphologies of waveguide 2; (c) top and side view morphologies of waveguide 3

对于轴向的倾斜角度设定为2°，由于中间芯到任一侧芯的中心距离为42 μm，因此波导长度约为1.203 mm。制备FBG和波导时，所使用的激光重复频率为100 kHz，脉冲功率（进入物镜前）分别为2.8 mW和2.3 mW，所使用的加工速度均为0.1 mm/s。

FBG及耦合波导的具体制备步骤如下：首先，将光纤夹持在旋转夹持器上，旋转光纤使纤芯1、3、6位于同一水平面且垂直于激光入射方向；接着，在core 1中制备一段周期为1.075 μm的FBG1；随后，将位移台沿$y$轴方向移动42 μm，将飞秒激光聚焦在core 3中，在与FBG1相同$x$方向起点位置处制备一段周期为1.07 μm的FBG3；然后，在FBG1起始点$x$方向后端2 mm处，利用逐行扫描法制备波导3；完成后，利用旋转夹持器将光纤顺时针旋转60°，在core 2中制备一段周期为1.065 μm的FBG2；最后，在FBG1起始点后端2.5 mm处，制备波导2。所制备的三个FBG的反射光谱如图5所示，该反射谱是在室温（25 ℃）环境下测量得到的，其中FBG1、FBG2、FBG3的初始中心波长分别为1555.53、1541.19、1548.60 nm。该反射光谱是将普通单模光纤与七芯光纤传感探头熔接，再将单模光纤连接到环形器，利用光谱分析仪测得的。这里，由于两个波导在$x$方向（光纤轴向）上的位置为一前一后，为了使FBG2和FBG3的反射光谱强度基本一致以便解调，需要控制两个波导的宽度，以尽量平衡输入光在侧芯2和侧芯3中的强度大小。由于波导2在波导3前面，因此波导2的宽度相对较小而波导3宽度较大。最终，波导2和波导3的宽度被分别设定为5.0 μm和7.5 μm。由于使用的激光脉冲功率和加工速度等参数相同，这两个波导在$z$轴方向上具有相同的厚度（约为5 μm），如图4(b)和图4(c)所示。

这里，FBG1的作用有两点：1）用于定位。方便在制备FBG2、FBG3及两个波导时，通过显微图像观察，

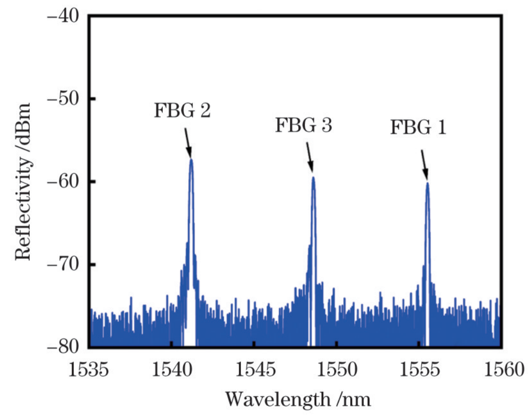


图5　光纤环形器测量得到的反射光谱

Fig. 5　Reflection spectra measured by fiber circulator

可以精确地定位各自的起始位置；2）用于温度补偿。当位移和温度变化同时作用于该传感结构时，由于中间纤芯对位移不敏感，通过监测该FBG的波漂可以补偿温度的变化，使得传感结构能够更加准确地测量位移变化。

另外，利用可调谐激光光源和黑白CCD探头测试了该传感结构的端面光出射情况。通入波长为1550.00 nm的输入光，在七芯光纤出射端的后方焦平面处进行CCD直接成像，结果如图6(a)所示。可以观察到端面只有三个纤芯出光，其中包括一个中间芯和两个方位角相差60°的侧芯，该结果初步验证了所制备的耦合波导具有良好的导光功能。然而，受限于该黑白CCD的探测精度，难以清晰地表征三个纤芯的实际模场强度分布。因此，利用另一激光光束分析仪的CCD探头及其配套的彩色成像激光光束分析软件，同样通入波长为1550.00 nm的输入光，测试了该结构的出射模场分布，结果如图6(b)和图6(c)所示。在该测试过程中，首先，通过旋转光纤，可以确定core 1的模场；其次，由于波导3的宽度（7.5 μm）接近纤芯，且比

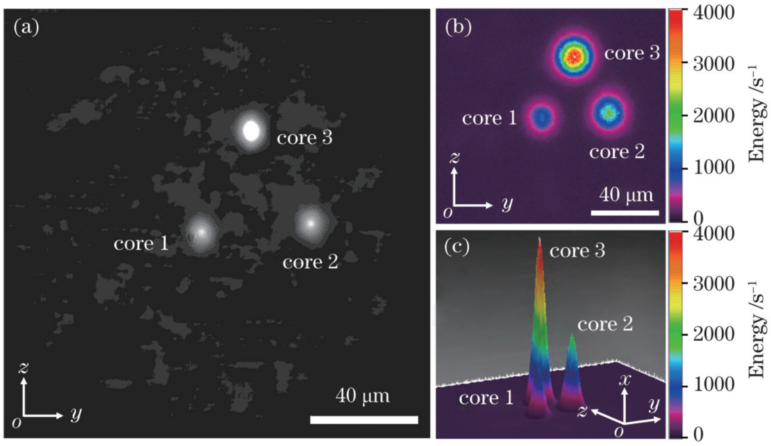


图6　通过黑白CCD成像和彩色激光光束分析仪得到的七芯FBG及耦合波导结构的端面出光分布。(a)黑白CCD成像结果；(b)彩色二维模场分布；(c)彩色三维模场分布

Fig. 6　End-side light distributions of seven-core FBG and coupled waveguide structure detected by monochrome CCD imaging and color laser beam profiler. (a) Monochrome CCD imaging result; (b) color two-dimensional mode field distribution; (c) color three-dimensional mode field distribution

波导2的宽度(5 μm)大很多[图4(b)、(c)],因此,模场强度大的侧芯为core 3,模场强度小的侧芯为core 2,这样就能最终确定三个纤芯的模场强度分布。

### 3.2 矢量位移传感测试

通过自行搭建的位移测试系统,测量了该传感结构对不同方向的位移响应。如图7所示,在室温为25 ℃的测试条件下,将传感结构探头的一侧(自由光纤长度为2 cm,光栅区域贴近左侧夹持端)固定在安装于一维手动线性位移台上的光纤旋转器(能够沿光纤径向改变位移方向)中,另一侧则是自由放置在光纤固定架上,并且其高度可以通过一个垂直升降台(分辨率为10 μm)改变。当平台在垂直方向上提供一定的位移时,传感光纤将出现相应的弯曲变形。为了避免对光栅周期的潜在影响以及大弯曲变形条件下FBG光谱可能出现的畸变,所施加的位移幅度相对较小。利用放大自发辐射(ASE)光源和光谱分析仪(OSA)表征了传感结构位移时的光谱响应。在一定的位移幅度下,传感FBG的反射波长在0°~360°(设置步长为10°)范围内呈近似正弦分布,如图8(a)所示。由该实验结果可知,所得的位移响应表现出一种方向依赖性,可以用来区分方向,正如我们在上文中所讨论的那样。另外,两个传感FBG在每个方向上对位移的响应不同,整体呈现出60°的相位差,正好对应两个FBG所处纤芯的方位角,这一点进一步提高了方向响应性。也就是说,该传感结构相当于集成了两个传感探头,可用于检测整个光纤径向($y$和$z$方向)的位移变化。

如图8(a)所示,此时FBG2和FBG3的最大位移灵敏度方向分别在210°和150°附近。因此,我们分别测量了这两个角度下传感结构的位移响应。图8(b)中$x$代表横轴量,$y_{\mathrm{FBG2}}$、$y_{\mathrm{FBG3}}$分别代表FBG2和FBG3的纵轴量,$R^2$为相关系数。可以得到该矢量位移传感结构在二维平面位移下的最大位移灵敏度约为0.28 nm/mm。

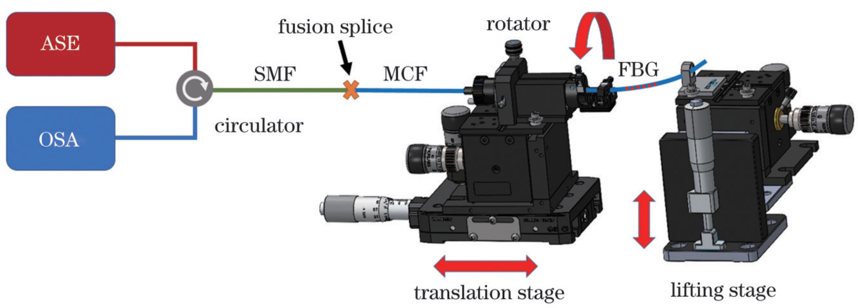


图7　位移测试系统示意图

Fig. 7　Schematic diagram of displacement measurement system

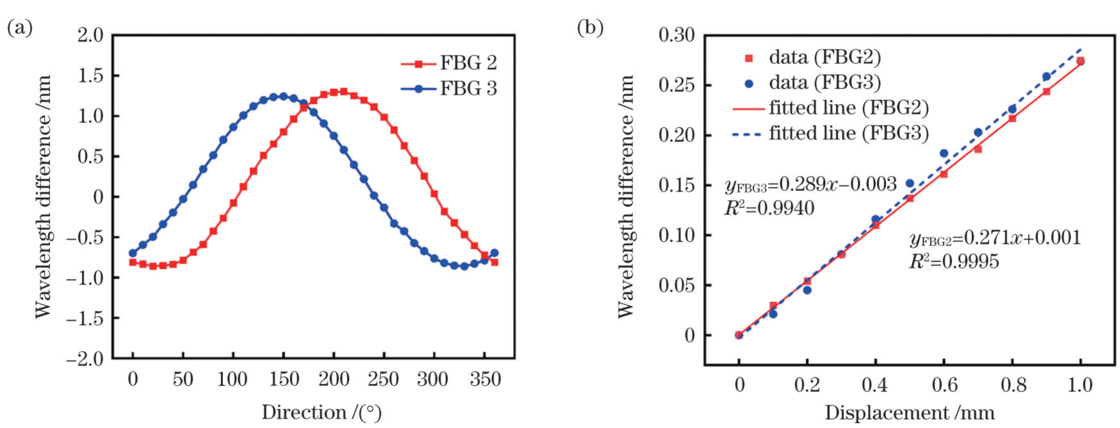


图8　FBG2和FBG3的方向响应以及在最灵敏方向角下的位移响应。(a)FBG2与FBG3在不同位移方向下的反射波长变化;(b)FBG2与FBG3在最大位移灵敏度方向下的位移响应

Fig. 8　Directional responses of FBG2 and FBG3 and their displacement responses under most sensitive directional angle. (a) Reflection wavelength differences of FBG2 and FBG3 under different displacement directions; (b) displacement responses of FBG2 and FBG3 in direction of maximum displacement sensitivity

随后,我们对该传感结构的位移方向进行了计算重构。首先,在位移量为0 mm、角度为0°时,记录下FBG2和FBG3的反射波长$\lambda_2$、$\lambda_3$并将其作为各自的初始波长;随后,设置位移量为3 mm,并以20°为步长,记录0°~360°范围内FBG2和FBG3的反射波长相对于其初始波长的变化量$\Delta\lambda_2$、$\Delta\lambda_3$;最后代入式(3)进行计算重构(这里$\theta_3$=0°,$\theta_2$=60°)。对该重构实验进行了三次重复测量,其平均重构结果如图9(a)所示。通过对该结果的数据点作线性拟合,可以看出该重构结果的线性度较高,重构出的位移方向与实际施加的位移方向较为吻合。图9(b)给出了三次重复测量时不同施加方向下重构出的各角度的平均误差,并给出了其误差范围。可以

看出，误差整体在±5°之间且普遍在±3°以内，该结果受限于光源、光谱仪波动导致的仪器误差以及手动旋转光纤旋转器时引入的实验误差，未来可通过更高精度的测试设备和测试方法来进一步提升测量精度。

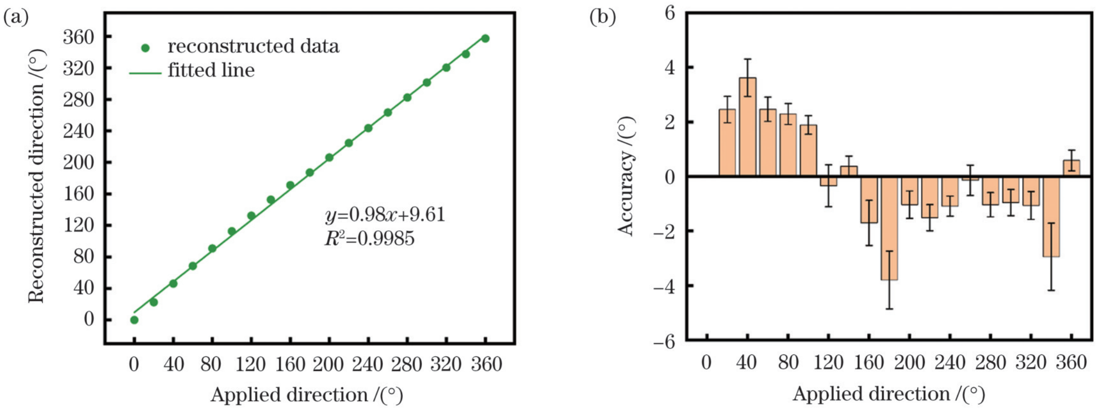


图9 三次重复测量下，位移方向的平均重构结果以及各个方向上的重构误差。(a)重构出的方向随施加的方向的变化；(b)不同施加方向下重构出的角度误差

Fig. 9 Average reconstruction results of displacement direction and reconstruction errors in each direction under three repeated measurements. (a) Reconstructed direction versus applied direction; (b) reconstructed angle errors under different applied directions

接着，为了研究传感结构的性能，对不同位移量下传感结构的方向响应进行了测试和比较。设置位移量为0.5～3.0 mm，步长为0.5 mm，分别以FBG2和FBG3各自在0 mm位移、0°方向时的波长作为初始波长，对比了传感结构在0°～360°（步长为10°）下的FBG2和FBG3的波长漂移量。利用该对比实验的结果，我们在直角坐标中绘制了FBG波长漂移量相对于光纤位移方向角的函数。如图10(a)和图10(b)所示，FBG2与FBG3的方向响应始终呈近似正弦分布，且整体相位差始终为60°。另外，还测试了传感结构在不同位移方向

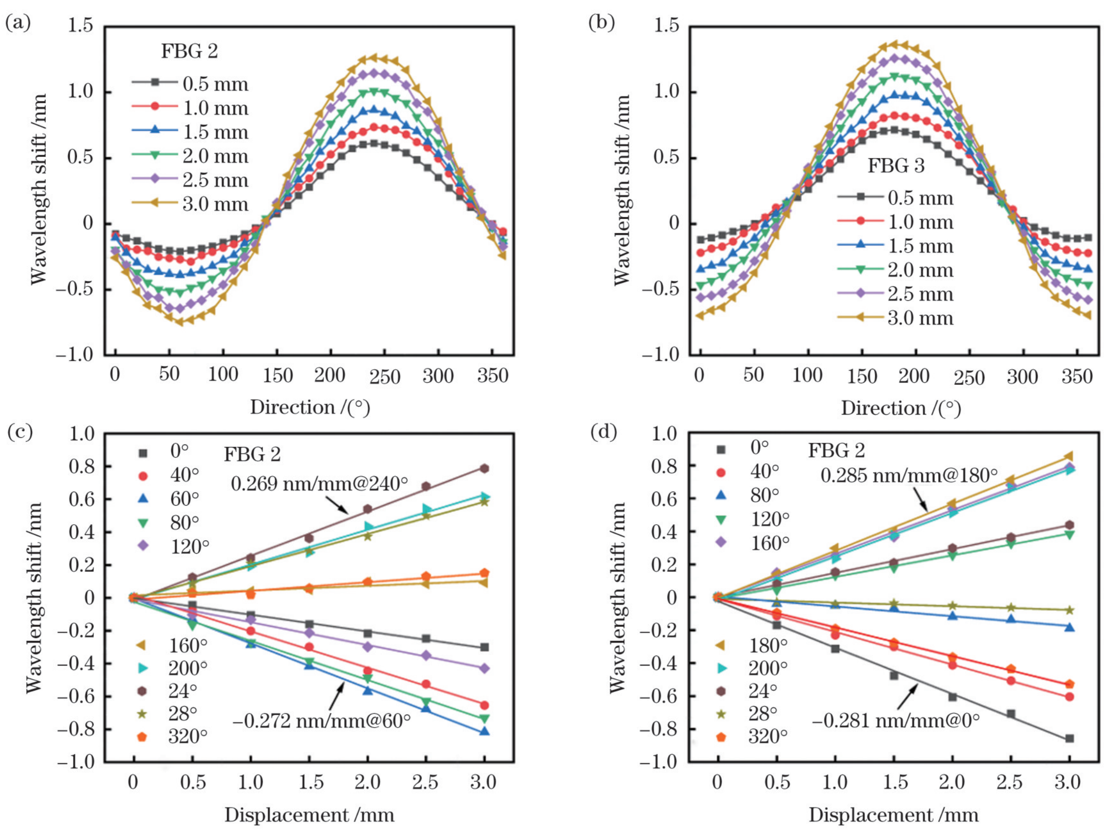


图10 位移方向及位移响应。(a)在不同位移量大小下FBG2的位移方向响应；(b)在不同位移量大小下FBG3的位移方向响应；(c)在不同位移方向下FBG2的位移响应；(d)在不同位移方向下FBG3的位移响应

Fig. 10 Displacement direction and displacement responses. (a) Displacement direction responses of FBG2 under different displacements; (b) displacement direction responses of FBG3 under different displacements; (c) displacement responses of FBG2 under different displacement directions; (d) displacement responses of FBG3 under different displacement directions

角下的位移灵敏度。如图10(c)和图10(d)所示,每40°为一组,测量了各个方向下FBG的位移响应,其中在两个FBG的最灵敏方向角处多测了一组数据(即FBG2的60°和FBG3的180°)。可以得到,FBG2在240°和60°位移方向角下的位移灵敏度分别为0.269 nm/mm和−0.272 nm/mm,FBG3在180°和0°位移方向角下的位移灵敏度分别为0.285 nm/mm和−0.281 nm/mm。

因此,该实验结果表明,对于光纤径向上发生的任意位移,都可以通过监测FBG2和FBG3的波长漂移,并进一步通过位移矢量合成的方法来确定该位移的方向和大小。该两组实验可以通过设置更多组不同大小的位移量和位移方向,并对每组位移量和位移方向下的波漂进行多次重复测量并求平均,从而实现更全面、准确的光纤径向全方位二维矢量位移传感。

## 4 结 论

提出了一种基于飞秒激光直写多芯FBG的二维矢量位移传感结构。通过在多芯光纤中使用飞秒激光直写的FBG和耦合波导,实现了单根纤芯复用多路传感光信号功能。该结构避免了常规扇入扇出器件的使用,降低了多芯FBG矢量位移传感系统的成本和复杂度,实现了高度集成。对FBG及耦合波导的设计和制备过程进行了讨论,确定了波导2和波导3的宽度分别为5.0 μm和7.5 μm,并对该传感结构的端面出光情况进行了测试,验证了所制备波导良好的导光性能。基于该传感结构,进行了0°~360°方向下的光纤径向二维矢量位移传感测试,并对位移方向角的测试结果进行了计算重构和误差分析。受限于测试设备的精度,方向角的重构误差整体在±5°以内。测试了传感结构在不同位移量大小下的位移方向响应,得到始终呈近似正弦分布的稳定响应效果,并测试了在不同方向角下的位移响应,得到传感结构的最大位移灵敏度约为0.28 nm/mm。实验结果表明,该传感结构通过监测FBG2和FBG3的波长漂移,并进一步通过位移矢量合成的方法,可以最终确定位移的方向和大小,实现二维矢量位移传感。该传感结构紧凑性良好,制备难度较低,未来有望应用于智能机械、形状监测、裂纹生长监测等领域。

## 参 考 文 献


[1] Leal-Junior A G, Frizera-Neto A, Pontes M J, et al. Hysteresis compensation technique applied to polymer optical fiber curvature sensor for lower limb exoskeletons[J]. Measurement Science and Technology, 2017, 28(12): 125103.

[2] Jang M, Kim J S, Um S H, et al. Ultra-high curvature sensors for multi-bend structures using fiber Bragg gratings[J]. Optics Express, 2019, 27(3): 2074-2084.

[3] Sun G K, Li H, Dong M L, et al. Optical fiber shape sensing of polyimide skin for a flexible morphing wing[J]. Applied Optics, 2017, 56(33): 9325-9332.

[4] 陈慧芳, 严惠民, 单国峰. 基于选择填充光子晶体光纤的二维弯曲矢量传感器设计[J]. 中国激光, 2016, 43(1): 0105003.
Chen H F, Yan H M, Shan G F. Design of two-dimensional bending vector sensor based on selective infiltration of photonic crystal fiber[J]. Chinese Journal of Lasers, 2016, 43(1): 0105003.

[5] 李俊, 张鼎博, 张新炜, 等. 基于光纤光栅传感与视频位移计技术的运营期铁路隧道结构安全监测[J]. 激光与光电子学进展, 2023, 60(23): 2312006.
Li J, Zhang D B, Zhang X W, et al. Safety monitoring of railway tunnel structure during operation period based on fiber grating sensing and video displacement meter technology[J]. Laser & Optoelectronics Progress, 2023, 60(23): 2312006.

[6] 郑勇, 余洁, 陈洪凯, 等. 基于光纤光栅的矢量位移测量传感装置与试验研究[J]. 光子学报, 2024, 53(2): 0206005.
Zheng Y, Yu J, Chen H K, et al. A vector displacement measurement sensing device based on fiber Bragg grating and its experimental study[J]. Acta Photonica Sinica, 2024, 53(2): 0206005.

[7] 朱晓亮, 虞瑶, 张晓东, 等. 融锥多芯光纤弯曲传感器[J]. 激光与光电子学进展, 2023, 60(7): 0728002.
Zhu X L, Yu Y, Zhang X D, et al. Bending sensor based on tapered multicore fiber[J]. Laser & Optoelectronics Progress, 2023, 60(7): 0728002.

[8] Kisała P, Harasim D, Mroczka J. Temperature-insensitive simultaneous rotation and displacement (bending) sensor based on tilted fiber Bragg grating[J]. Optics Express, 2016, 24(26): 29922-29929.

[9] Chen X F, Zhang C, Webb D J, et al. Highly sensitive bend sensor based on Bragg grating in eccentric core polymer fiber[J]. IEEE Photonics Technology Letters, 2010, 22(11): 850-852.

[10] Feng D Y, Qiao X G, Albert J. Off-axis ultraviolet-written fiber Bragg gratings for directional bending measurements[J]. Optics Letters, 2016, 41(6): 1201-1204.

[11] Chen F Y, Li X Y, Wang R H, et al. Two-dimensional vector accelerometer based on orthogonal Bragg gratings inscribed in a standard single-mode fiber cladding[J]. Optics Letters, 2021, 46(12): 2992-2995.

[12] Kong J, Ouyang X W, Zhou A, et al. Pure directional bending measurement with a fiber Bragg grating at the connection joint of eccentric-core and single-mode fibers[J]. Journal of Lightwave Technology, 2016, 34(14): 3288-3292.

[13] Osório J H, Oliveira R, Aristilde S, et al. Bragg gratings in surface-core fibers: refractive index and directional curvature sensing[J]. Optical Fiber Technology, 2017, 34: 86-90.

[14] Zhao D H, Chen X F, Zhou K M, et al. Bend sensors with direction recognition based on long-period gratings written in D-shaped fiber[J]. Applied Optics, 2004, 43(29): 5425-5428.

[15] Yin X L, Zhou R X. Compact vector fiber-optic displacement sensor using an asymmetric Mach - Zehnder interferometer[J]. Optics Communications, 2017, 400: 74-78.

[16] Wang Q, Liu Y. Review of optical fiber bending/curvature sensor[J]. Measurement, 2018, 130: 161-176.

[17] Frazão O, Viegas J, Caldas P, et al. All-fiber Mach-Zehnder curvature sensor based on multimode interference combined with a long-period grating[J]. Optics Letters, 2007, 32(21): 3074-3076.

[18] Shao L Y, Laronche A, Smietana M, et al. Highly sensitive bend sensor with hybrid long-period and tilted fiber Bragg grating[J]. Optics Communications, 2010, 283(13): 2690-2694.

[19] Hou M X, Yang K M, He J, et al. Two-dimensional vector bending sensor based on seven-core fiber Bragg gratings[J]. Optics Express, 2018, 26(18): 23770-23781.

[20] Cui J X, Gunawardena D S, Liu Z Y, et al. All-fiber two-dimensional inclinometer based on Bragg gratings inscribed in a seven-core multi-core fiber[J]. Journal of Lightwave Technology, 2020, 38(8): 2516-2522.

[21] Yang K M, He J, Liao C R, et al. Femtosecond laser inscription of fiber Bragg grating in twin-core few-mode fiber for directional bend sensing[J]. Journal of Lightwave Technology, 2017, 35(21): 4670-4676.

[22] Flockhart G M H, MacPherson W N, Barton J S, et al. Two-axis bend measurement with Bragg gratings in multicore optical fiber[J]. Optics Letters, 2003, 28(6): 387-389.

[23] An M W, Geng T, Yang W L, et al. A direction detective asymmetrical twin-core fiber curving sensor[J]. Proceedings of SPIE, 2015, 9679: 967910.

[24] Wang S, Zhang W G, Chen L, et al. Two-dimensional microbend sensor based on long-period fiber gratings in an isosceles triangle arrangement three-core fiber[J]. Optics Letters, 2017, 42(23): 4938-4941.

[25] 张鹏浩, 武洪波, 陈爽, 等. 基于小孔径光阑整形的低损耗飞秒光纤光栅制备[J]. 中国激光, 2024, 51(2): 0206003.
Zhang P H, Wu H B, Chen S, et al. Fabrication of low-loss femtosecond fiber bragg gratings based on beam shaping by small aperture[J]. Chinese Journal of Lasers, 2024, 51(2): 0206003.

[26] Chen L, Fu C L, Cai Z H, et al. High-quality fiber Bragg grating inscribed in ZBLAN fiber using femtosecond laser point-by-point technology[J]. Optics Letters, 2022, 47(14): 3435-3438.

[27] Cai Z H, Li B Z, Bai Z Y, et al. Encrypted optical fiber tag based on encoded fiber Bragg grating array[J]. International Journal of Extreme Manufacturing, 2023, 5(3): 035502.

[28] 王士香, 陈志翔, 刘洪亮, 等. 飞秒激光直写Tm:YAP波导脉冲激光器[J]. 光学学报, 2023, 43(16): 1623018.
Wang S X, Chen Z X, Liu H L, et al. Tm: YAP waveguide pulsed lasers of femtosecond laser direct writing[J]. Acta Optica Sinica, 2023, 43(16): 1623018.

[29] 李文春, 肖凯恒, 李中天, 等. 大曲率低损耗弯曲波导的飞秒激光直写[J]. 中国激光, 2024, 51(16): 1602403.
Li Y C, Xiao K H, Li Z T, et al. Femtosecond laser direct writing of bent waveguides with high curvature and low loss[J]. Chinese Journal of Lasers, 2024, 51(16): 1602403.

[30] Waltermann C, Doering A, Köhring M, et al. Cladding waveguide gratings in standard single-mode fiber for 3D shape sensing[J]. Optics Letters, 2015, 40(13): 3109-3112.

[31] Zou M Q, Liao C R, Chen Y P, et al. 3D printed fiber-optic nanomechanical bioprobe[J]. International Journal of Extreme Manufacturing, 2023, 5(1): 015005.

[32] Hearn E J. Mechanics of materials. 2: the mechanics of elastic and plastic deformation of solids and structural materials[M]. 3rd ed. Oxford: Butterworth-Heinemann, 1997.

[33] Kersey A D, Davis M A, Patrick H J, et al. Fiber grating sensors [J]. Journal of Lightwave Technology, 1997, 15(8): 1442-1463.

# Two-Dimensional Vector Displacement Sensing Based on Femtosecond Laser Direct-Writing Multicore Fiber Bragg Grating and Coupled Waveguides

Fan Yu[1,2,3], Bao Weijia[1,2,3*], Liao Changrui[1,2,3], Wang Yiping[1,2,3,4]

[1]*State Key Laboratory of Radio Frequency Heterogeneous Integration, Shenzhen University, Shenzhen* 518060, *Guangdong, China;*

[2]*Guangdong and Hong Kong Joint Research Centre for Optical Fiber Sensors, Shenzhen University, Shenzhen* 518060, *Guangdong, China;*

[3]*Shenzhen Key Laboratory of Ultrafast Laser Micro/Nano Manufacturing, Shenzhen University, Shenzhen* 518060, *Guangdong, China;*

[4]*Guangdong Laboratory of Artificial Intelligence and Digital Economy (Shenzhen), Shenzhen* 518107, *Guangdong, China*

## Abstract

**Objective** In recent years, multicore fiber Bragg grating (FBG) vector displacement sensors have become a research hotspot in the field of vector displacement sensing because of their multidimensional measurement capability, high sensitivity, high resolution, and high precision. However, in practical applications, multicore FBG vector displacement sensors require a fan-in and fan-out device to realize multichannel signal demodulation. The use of this device not only increases the difficulty of fiber fusion splicing and reduces the compactibility of the sensor but also increases the cost and complexity of the system and reduces modulation efficiency, which poses a challenge to the practical application of the existing multicore FBG vector displacement sensor. In this study, a vector displacement sensing structure based on multicore FBGs and coupled waveguides is proposed, to measure multiple signals in a single channel and avoid the use of fan-in and fan-out device.

**Methods** First, for preparation, a sensing structure was studied. FBGs were inscribed in the central core (core 1) and two outer cores (core 2 and core 3) with an azimuth difference of 60° for a seven-core fiber, using femtosecond laser direct-writing technology. In addition, straight coupled waveguides for connecting core 1 to core 3 and core 1 to core 2 were prepared, to enable signal light transmission back and forth between the central and outer cores. Figure 2 shows the principle of multiplexing multichannel sensing signals, using a single core based on this structure. Subsequently, the principle of displacement sensing based on multicore FBGs was theoretically analyzed. Finally, based on the self-built displacement testing system (Fig. 7), a displacement-sensing test was performed on the prepared sensing structure, to verify its performance.

**Results and Discussions** Femtosecond laser direct writing technology was used to prepare a reference FBG (FBG1) for auxiliary positioning and temperature compensation in core 1, and a sensing FBG (FBG2 and FBG3) for detecting displacement changes in core 2 and core 3. The lengths of FBG1–FBG3 were 5 mm. Subsequently, two coupled waveguides for connecting core 1 & core 2 (waveguide 2) and core 1 & core 3 (waveguide 3) were prepared using line-by-line technology. Waveguide 2 was located upstream of the fiber with a width of 5 μm, whereas waveguide 3 was located downstream with a width of 7.5 μm. The reason for the different widths of the two waveguides was to make the reflection intensities of FBG2 and FBG3 closer to facilitate demodulation. Finally, the reflection spectra of FBG1–FBG3 measured by a single-mode fiber circulator (Fig. 5) show that the reflection intensity of the three FBGs were basically close to being the same. The end-side light distribution (Fig. 6) shows that the prepared coupled waveguides exhibit good light-conduction performance. Subsequently, a displacement sensing test was performed based on the displacement testing system (Fig. 7). First, the directional response of the sensing structure in the direction angle of 0–360° was tested in 10° increments, verifying that the directional response of this sensing structure approximately follows a sinusoidal distribution [Fig. 8(a)]. The phase difference between FBG2 and FBG3 was 60°, which is consistent with the theoretical analysis results. In addition, the displacement response under the most sensitive direction angle was tested, verifying a maximum displacement sensitivity of approximately 0.28 nm/mm. Subsequently, the directional response was reconstructed to verify the accuracy of the sensing structure in detecting the displacement direction. After three repeated measurements (0–360°, in increments of 20°), the corresponding relationship between the applied angle and average calculated reconstructed angle was obtained [Fig. 9(a)]. From the linear fitting of the reconstruction angle, the actual applied direction was observed to be in good agreement with the calculated reconstruction result. Moreover, the average reconstruction errors of each angle in three repeated experiments were measured, and the overall error range was within ±5° [Fig. 9 (b)]. Finally, to investigate the performance of the sensor structure in detail, additional groups of the directional and displacement responses of FBG2 and FBG3 were tested. The directional response of FBG2 and FBG3 (0–360°, in increments of 10°) for a displacement range of 0.5–3.0 mm [Figs. 10 (a) and (b)] and the displacement response of FBG2 and FBG3 (0–3 mm, with a step of 0.5 mm) in all directions (0–360°, in increments of 40°) were tested. The results indicate that the direction and magnitude of any displacement can be determined by monitoring the wavelength shifts of FBG2 and FBG3, using displacement vector synthesis. By setting more groups of displacements and directions and averaging the FBG wavelength shift in each group, more comprehensive and accurate two-dimensional vector displacement sensing can be achieved in the fiber radial direction.

**Conclusions** This study demonstrates a novel single-channel measurement multicore FBG vector-displacement sensing structure. Using femtosecond laser direct-writing FBGs and coupled waveguides in multicore fibers, the multiplexing of multichannel signals was realized in a single core. This structure avoids the use of conventional fan-in and fan-out devices, reduces the cost and complexity of multicore FBG vector-displacement sensing systems, and realizes a highly integrated sensing structure. The design and fabrication processes of FBGs and coupled waveguides are discussed. The widths of waveguide 2 and waveguide 3 were determined to be 5.0 μm and 7.5 μm, respectively. The end-side light distribution of the structure verified the satisfactory light conduction performance of the waveguide. Two-dimensional vector displacement sensing in the direction of 0–360° was subsequently tested based on this structure, and the results of the reconstructed direction indicated the directional accuracy of this sensing structure. Finally, the direction response of the structure under different displacement sizes was tested, verifying a series of stable responses that followed an approximate sinusoidal distribution. The displacement responses at different direction angles were also tested, and the maximum displacement sensitivity of the structure was approximately 0.28 nm/mm. The experimental results show that by monitoring the wavelength shift of FBG2 and FBG3 and by further employing the method of displacement vector synthesis, such a structure can finally determine the direction and magnitude of displacement and realize two-dimensional vector displacement sensing. Such a sensing structure has good compactibility and low preparation difficulty, making it applicable to intelligent machinery, shape monitoring, crack growth monitoring, and other fields in the future.

**Key words** vector displacement sensing; femtosecond laser direct writing; multicore fiber; fiber Bragg grating; waveguide